Electron microscopy studies of the thermal stability of gold nanoparticle arrays

Roger Ristau*, Ramchandra Tiruvalam, Patrick L. Clasen, Edward P. Gorskowski, Martin P. Harmer and Christopher J. Kiely#,Center for Advanced Materials and Nanotechnology, Lehigh University, 5 East Packer Avenue, Bethlehem, PA 18015-3195, USA.**
Irshad Hussain* and Mathias Brust Center for Nanoscale Science, Department of Chemistry, University of Liverpool, Liverpool, Merseyside, L69 3BX, UK.**

* Now at: Institute of Materials Science, University of Connecticut, Storrs, CT 06269, USA.
** Now at: Naval Research Laboratory, Multifunctional Materials Branch, Washington, DC 20375, USA.
*** LUMS School of Science and Engineering (SEE), D.H.A. Lahore Cantt – 54792, Pakistan.
# Corresponding author; E-mail: chk5@lehigh.edu Phone: (610) 758 4291

Abstract

A series of monolayer protected gold nanoparticle colloidal solutions have been prepared with average sizes in the 2-15nm range. If a drop of such a colloidal suspension is deposited onto a Si_3N_4 substrate and the solvent allowed to evaporate, the particles have a tendency to self-assemble into monolayer rafts with varying degrees of structural order depending on the initial mono-dispersity of the particles. The thermal stability of these self-assembled gold nanoparticle rafts as a function of particle size, heating method, heating rate and ligand identity have been assessed in this study. *In-situ* TEM studies show that sub-8nm Au nanoparticles on Si_3N_4 have a tendency to coarsen upon slow heating, whereas those comprised of larger particles exhibit densification. Increasing the heating rate for the smaller particles promoted densification, forcing them to form highly interconnected string-like structures. Finally, rafts of sub-4nm alkanethiol protected Au nanoparticles are shown to sinter spontaneously under ambient conditions at room temperature on the timescale of several months. This unexpected effect may have important implications for the long term structural stability of any device constructed from sub-4nm gold nanoparticles.

Introduction

To date the most successful approaches to nanoscale manipulation have been based on electron beam lithography [1] and scanning probe microscopy [2, 3]. Unfortunately these methods are relatively expensive, serial in nature, and are not readily applicable to the mass production of nano-engineered materials. The ability to reproducibly produce ordered nanostructures on a larger scale by inexpensive chemical methods is therefore of great practical importance [4, 5], especially if the promised potential benefits of nanotechnology are to be exploited in the next generation of consumer devices, chemical sensing devices and magnetic recording media. One of the most straightforward approaches for constructing ordered nanoparticulate superstructures is by drop-cast self-assembly, whereby a colloidal suspension of sterically stabilized nanoparticles is introduced at a substrate surface and the carrier medium allowed to evaporate in a controlled fashion. For particles with a sufficiently narrow monomodal size distribution, well-defined packing order tends to develop in monolayer films [6-11]. One of the most commonly used nanomaterials being exploited for this particular purpose are alkanethiol protected gold nanoparticles [6, 12].

An important factor which has received relatively scant attention to date is the thermal stability of such self-assembled nanoparticulate materials. Thiol-derivatised Au clusters are known to be stable in toluene for periods of many years. However, when the solvent is evaporated off and the particles are crystallized onto a substrate, the structural stability of the particles can be deliberately compromised. For instance, subjecting the particles to intense electron beam irradiation in the TEM can be sufficient to disrupt the protective alkanethiol coating [13]. Once this has occurred it becomes energetically favorable for the Au particles to reduce their surface energy by sintering. Alternatively, nanostructure destabilization may unexpectedly occur due to variations in ambient environmental storage conditions (e.g. elevated temperature, or exposure to solvent vapors) which may potentially disturb the protective ligand environment that are separating neighboring nanoparticles. The destabilization and sintering of these self-assembled structures can therefore be considered as a desirable or an adverse phenomenon depending on the particular circumstances. In many cases, where it is imperative to preserve the integrity of the nanoparticles within the self-assembled structure in order to exploit the size-dependant properties of its constituents in a

Figure 1

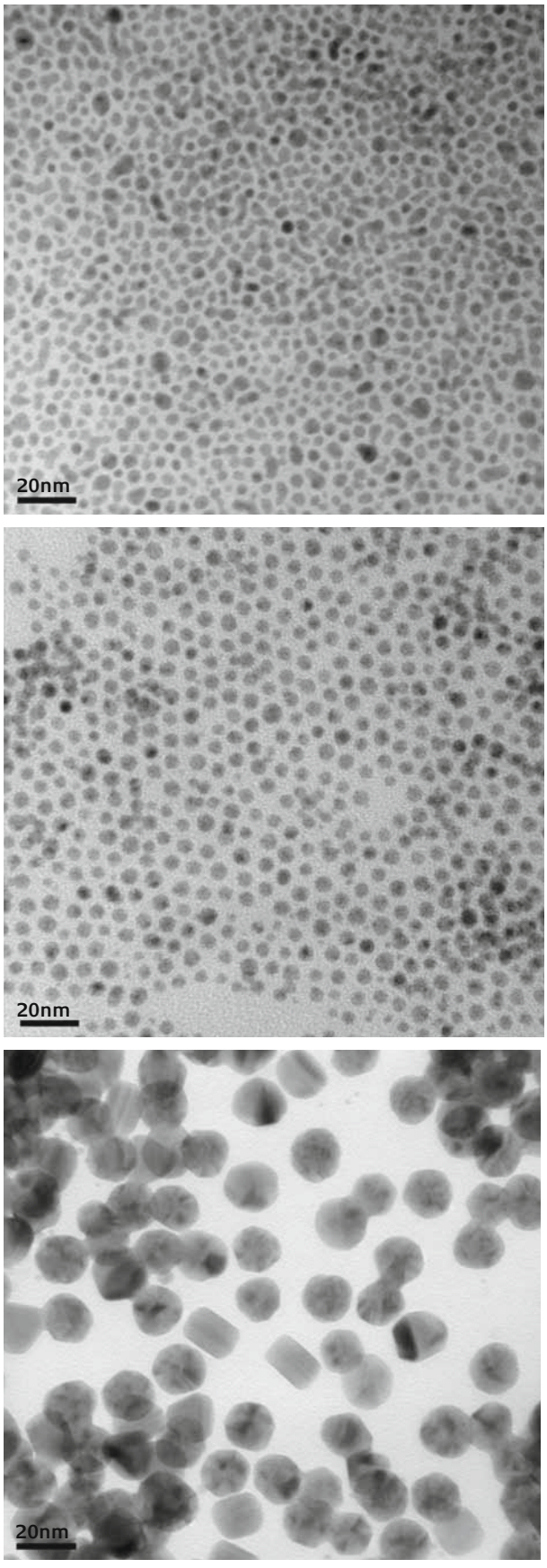

Representative transmission electron micrographs and corresponding histograms of particle size distribution for the nominal 4, 5 and 15nm preparations of Au nanoparticles

device, sintering will be a destructive nuisance. In other situations, where it may be beneficial to deliberately destabilize the self-assembled particles to form features such as nanowires, multilayer stacks or complex nanopatterns, sintering can be considered as a controllable processing step in a nano-manufacturing process [14, 15]. Being able to control both these scenarios depends on developing a basic understanding of the way in which nanoparticles held in such close proximity will sinter under a range of processing or storage conditions. In this paper we report some basic experiments to observe sintering phenomena for arrays of ligand stabilized gold nanoparticles in the 2-15nm size range.

Buffat and Borel have performed fundamental studies to determine the size-dependence of the melting point of bare gold nanoparticles [16, 17]. They used a heating stage in a transmission electron microscope and estimated the nanoparticle melting point from the temperature at which electron diffraction rings, and hence crystalline structure, disappeared. This pioneering work led to significant activity in studying the thermodynamics of melting of bare nanoparticles [18-20]. A number of subsequent *in-situ* transmission electron microscopy studies have also shed light of the structural stability [13, 21], evaporation [22] and coalescence [23, 24] characteristics of randomly arranged bare Au nanoparticles on carbon, HOPG and silica support films. These coalescence studies in particular have spawned a number of papers [24-29] where molecular dynamics calculations have been used to model the coalescence behavior of touching gold nanoparticles with clean surfaces.

In this work we have made a series of stock Au nanoparticle preparations in the range 2-15 nm and self-assembled them into two-dimensional arrays. We have then studied their destabilization and sintering behavior as a function of particle size and heating rate. A size regime is also identified where nanoparticles have a propensity to sinter spontaneously under dry ambient conditions at room temperature.

Experimental

Stock toluene solutions of dodecane-thiol capped Au nanoparticles of well-defined sizes (nominally 2, 3, 4, 5 & 8 nm) were prepared using a well-established synthesis method [30, 12]. For each stock solution, TEM images were acquired and histograms of nanoparticle sizes were generated in order to confirm that our target average particle size had been produced (see Figure 1). In addition, a solution of 15nm diameter Au nanoparticles were prepared in water by an acrylate reduction method developed at the University of Liverpool [31].

Si_3N_4 membranes were used as electron transparent supports for the nanoparticles since in sintering experiments they gave more easily interpretable results than those supported on conventional carbon thin films. For the latter type of membranes there are strong secondary Van der Waals type interactions between the rough amorphous C surfaces of a TEM support grid and the C_{10} hydrocarbon chains that make up the protective ligand molecules around the nanoparticles. Furthermore, the continuous C films were prone to carbon loss, perforation and eventual disintegration during heating experiments above 200°C, whereas the Si_3N_4 membranes were found to be much more robust at elevated temperatures. The nanoparticle assemblies were examined in either a Philips 420T TEM operating at 120kV or a JEOL 2000FX TEM operating at 200kV. A number of nanoparticle sintering methods were explored during the course of this work including, *ex-situ* furnace heating, *ex-situ* plasma heating, *in-situ* electron beam irradiation and *in-situ* conductive heating in a Philips annular TEM heating stage. Thermo-gravimetric analysis (TGA) studies were carried out using a Netzsch STA409 system.

Results and discussion

In order to investigate whether or not we were dealing with the sintering behavior of clean or ligand capped nanoparticles in our experiments some thermogravimetric analysis (TGA) measurements were carried out on a series of dried Au nanoparticles of various sizes to determine the temperature at which ligand de-stabilization occurred. Figure 2 shows comparative TGA traces for the 5nm and 15nm Au nanoparticle preparations respectively. The 2, 3, 5 and 8 nm particles, which were all dodecane-thiol capped, showed very

Figure 2

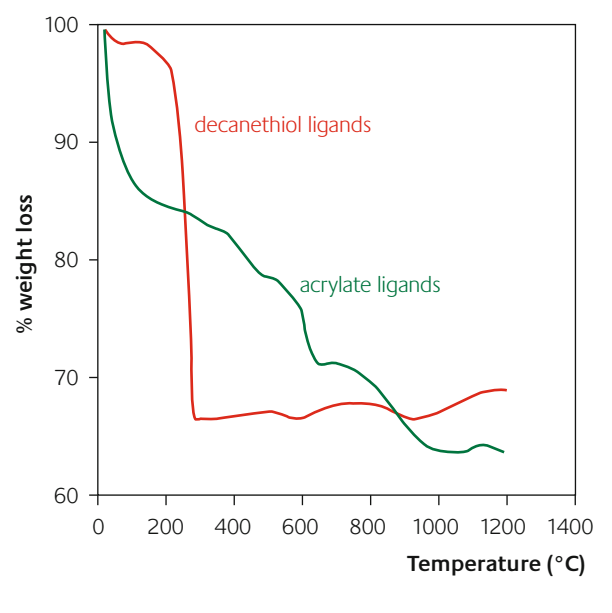

Comparative TGA traces obtained from 5nm dodecane-thiol capped Au nanoparticles and 15nm sodium acrylate capped Au nanoparticles

Figure 3

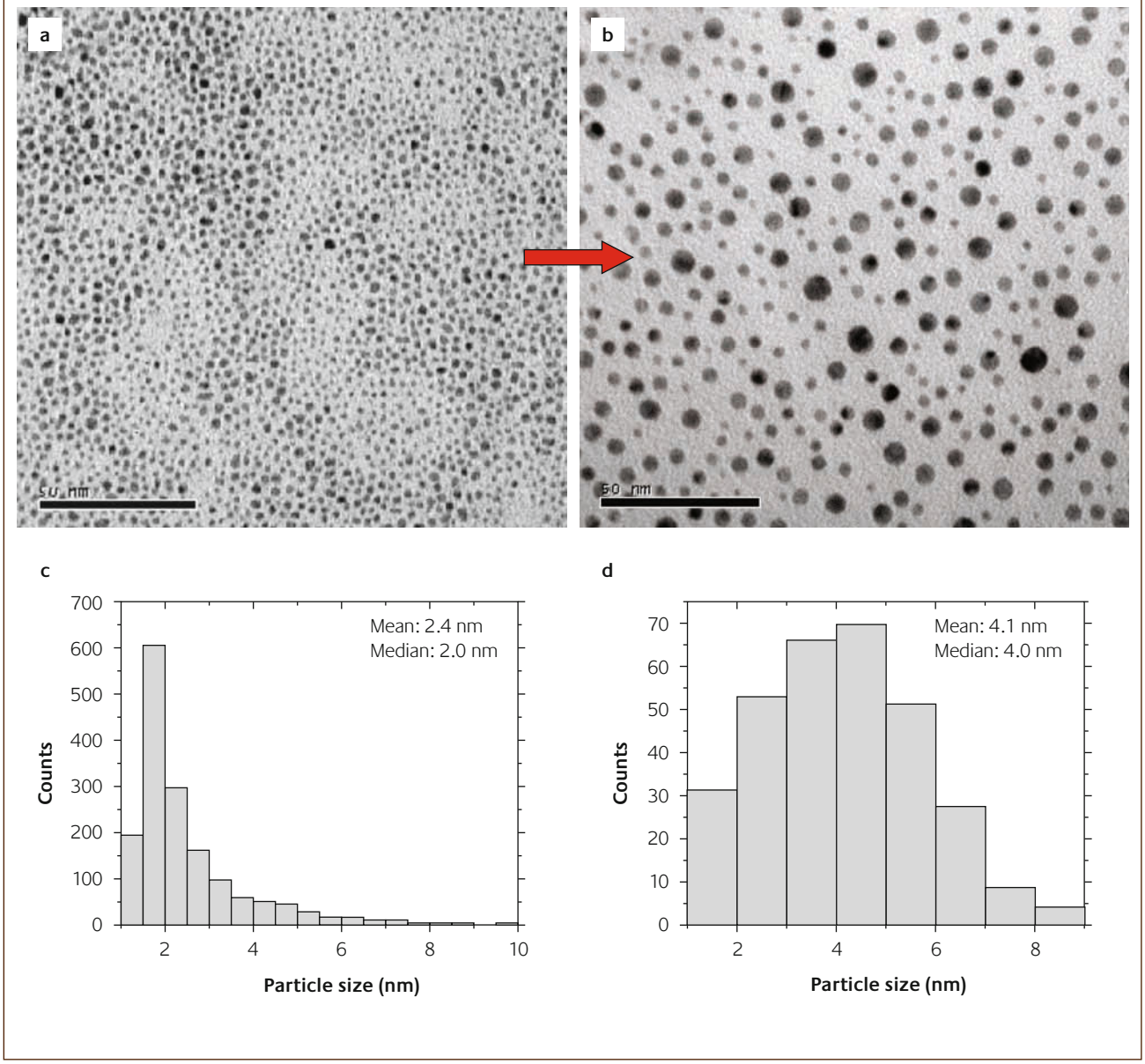

2 nm particles supported on Si_3N_4 (a) before and (b) after sintering [for 10 minutes at 250 ± 20°C in an annular TEM heating stage] showing classic coarsening behavior. The corresponding particle size distributions before and after sintering are shown in (c) and (d) respectively

similar behavior with a very small weight loss (<2%) around 100°C due to the desorption of water followed by a much more significant and sharp weight loss (about 33% for the 5nm preparation) in the range 220-260°C that corresponds to the clean desorption of the protective ligands as dithiol entities. This desorption behavior is consistent with previous TGA studies [32-34] where maximal ligand loss was noted at ~250°C, close to the boiling range (266-283°C) of neat dodecane-thiol. The 15nm particles on the other hand showed a slow gradual weight loss over the entire 100-1000°C temperature range which corresponds to a much more gradual desorption of the protective sodium acrylate groups. Hence we can be confident that our Au nanoparticles up to 8nm in diameter are clean if heated above 250°C, but the 15nm particles always contained residual ligands on their surfaces at the sintering temperatures used in our experiments.

Samples consisting of the smallest nanoparticles supported on Si_3N_4, such as the 2 nm particles shown before sintering in Figure 3(a), were observed to coarsen during *in-situ* sintering (i.e. some larger particles grow at the expense of smaller ones). Figure 3(b) shows an image of the 2 nm sample after ~10 minutes of sintering at 250 ± 20°C in the annular TEM heating stage. Clearly the mean and median particle size increased to ~4 nm while the total number of particles dramatically decreased. The corresponding particle size distributions are shown in Figure 3(c) and (d) respectively, where it is apparent that the shape of the distribution has

Figure 4

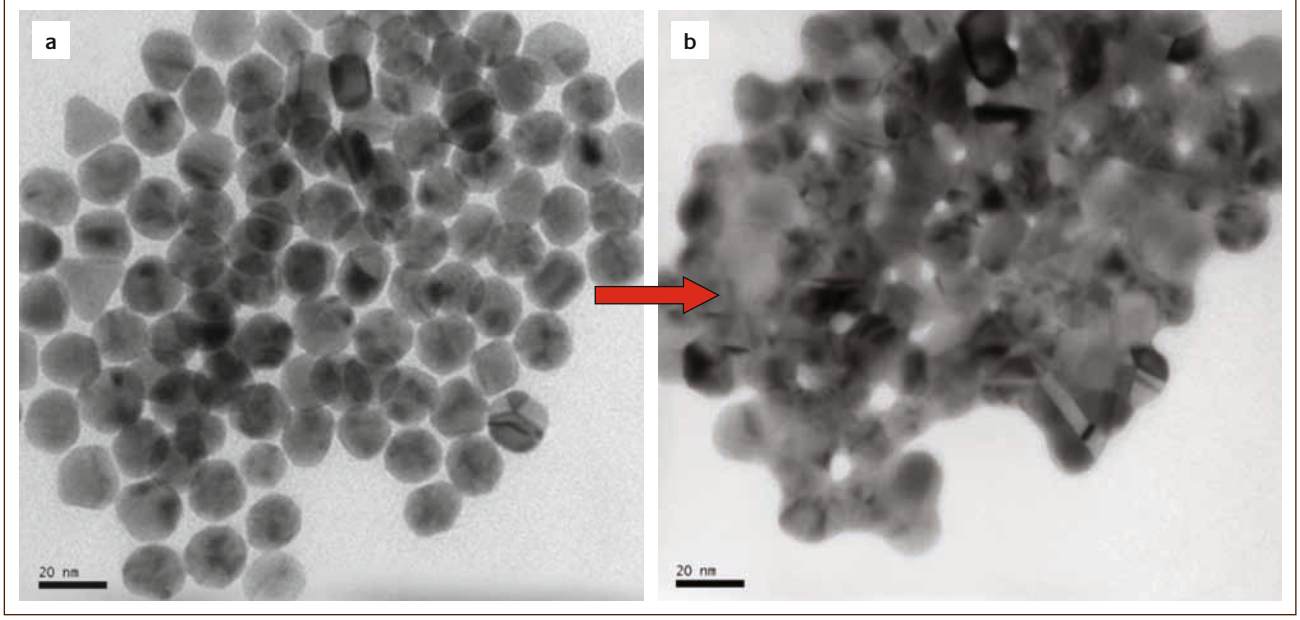

15 nm particles supported on Si_3N_4 before and after sintering [for 10 minutes at 250 ± 20°C in an annular TEM heating stage] showing classic densification behavior

also been modified slightly. The initial skewed distribution has become more Gaussian in character because of the more rapid sintering of the very smallest particles as compared to the larger ones, due to their greater melting point depression (as discussed later). Similar coarsening behavior was also observed for the 3, 4, 5 and 8 nm nanoparticle samples on Si_3N_4 membranes.

For the larger particles with a nominal size of 15 nm, densification, whereby the particle centers move closer to each other, was observed during sintering on Si_3N_4 regardless of the heating method. Figure 4(a) shows a TEM micrograph of Au particles with a measured mean size before sintering of ~17 nm (nominal 15 nm), and Figure 4(b) shows the same region after 14 minutes of *in-situ* sintering. Shrinkage of the nanoparticle agglomerate, and a decrease in pore size (densification) with a small amount of concurrent grain growth, as seen in Figure 4(b), was typical in this sample following both *in-situ* and *ex-situ* sintering.

The densification behavior for the 17 nm case may be related to the continued presence at the sintering temperature of the acrylate ligands, which are more strongly bound to the gold surface. By way of contrast, the 2, 3, 4, 5 and 8 nm particles, which all coarsened, were capped with alkanethiol ligands, which our TGA analyses (Figure 2) confirm to be volatile at the sintering temperature. Another fact that should be considered is that the ratio of the particle radius, R, to particle separation, S, are also varying significantly (*i.e.* $1 < R/S < 8$) in the complete set of samples examined. In the regime where R and S are comparable (*i.e.* $R/S < 4$) it may be difficult to get enough inter particle–particle contact to allow densification to proceed. Further systematic experiments are currently underway in which we are attempting to separate the effects of residual strongly bound ligands and the R/S ratio on the sintering mode observed.

Sintering was also induced locally in the nanoparticle arrays by condensing the 200keV electron beam generated from a LaB_6 filament in a JEOL 2000FX TEM down to a 300nm diameter convergent spot, and observing the effects of the beam on the nanoparticle raft. The condensed beam, supplying a current density of 50pA/nm^2, was held for 1 minute after which the beam intensity was decreased to normal level and an image recorded. This process was repeated in order to build up a time-sequence of images that captured the various stages on the sintering process in action.

Samples heated by the convergent electron beam showed sintering behavior very similar to that of the annular *in-situ* TEM heating stage, however, only within the local region affected by the high intensity beam. This similarity in sintering behavior is reasonable if one considers the likely interactions of the high incident electrons with the nanoparticle arrays supported on a Si_3N_4 membrane. The nanoparticles are not in particularly good thermal contact with Si_3N_4 membrane or each other, hence their temperature is likely to increase significantly by phonon excitation during electron beam irradiation, although it is very difficult to measure or estimate the precise temperature reached. The gold cores will not suffer significant knock-on damage under our illumination conditions, but it is highly probable that the ligands will suffer some radiolysis damage which would contribute to chain scission and eventual ligand desorption.

An advantage of the electron beam irradiation heating method was that it conveniently allowed a detailed evolutionary history of particle growth during sintering to be

Figure 5

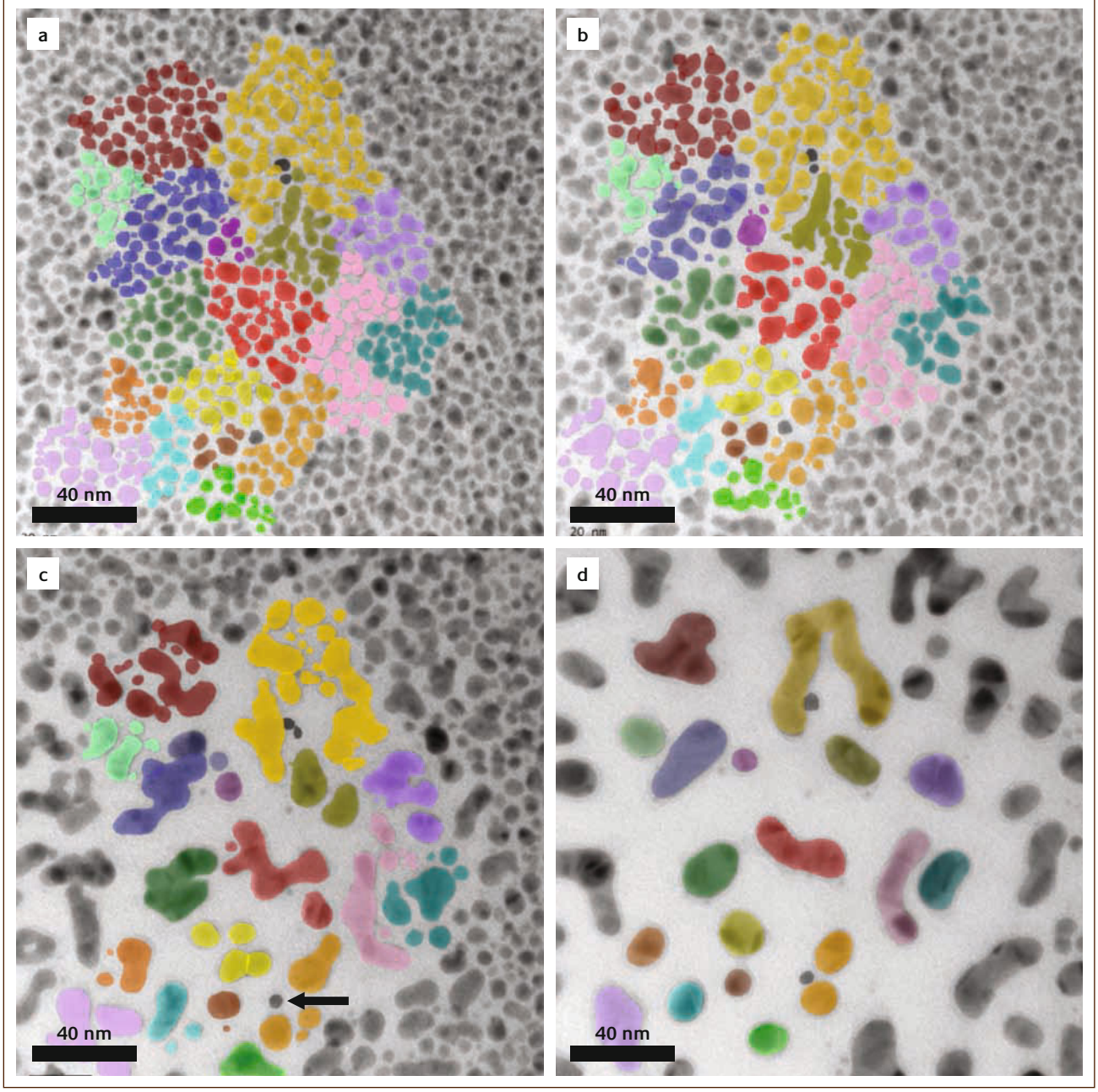

Sequence of micrographs showing the in-situ coarsening behavior of the 3nm particle preparation supported on a Si_3N_4 membrane. The images, which have been false colored to highlight nanoparticle trajectories, were captured after (a) 1 min, (b) 8 min, (c) 18 min and (d) 40 min of electron beam exposure [to a 300nm diameter spot with a current density of 50pA/nm^2]

recorded. For example, Figure 5 shows a time sequence of images showing the coarsening behavior of the 3nm particle preparation. Color coding has been used in Figures 5(a), (b) and (c) to highlight those particles which coalesce by surface diffusion and coarsen to the final particle configuration seen in Figure 5(d). Over the 40 minute beam exposure time of the experiment, all the particles (typically 40-80) shaded a particular color in an area of ~400 nm^2 are seen to coarsen into large single particles surrounded by a significant denuded zone. Considerable nanoparticle mobility was observed in such sequences, particularly in the early stages of the process where the particle mass was lowest.

Figure 6 shows a plot of mean particle size versus time derived from an irradiated region initially having about 2000 particles of ~3nm mean size. Coarsening progressed to reach a maximum projected mean diameter of 17 nm after 20 minutes of *in-situ* sintering, and then decreased in mean diameter to 14 nm after ~50 minutes. The decrease in diameter, assuming the particle volume remained constant, suggests that the particles were de-wetting the Si_3N_4 surface and becoming more spherical.

Occasionally some particles in the images (*e.g.* see the arrowed particle in Fig 5(c)) appear to remain unchanged while all those around are consumed by neighboring growing

Figure 6

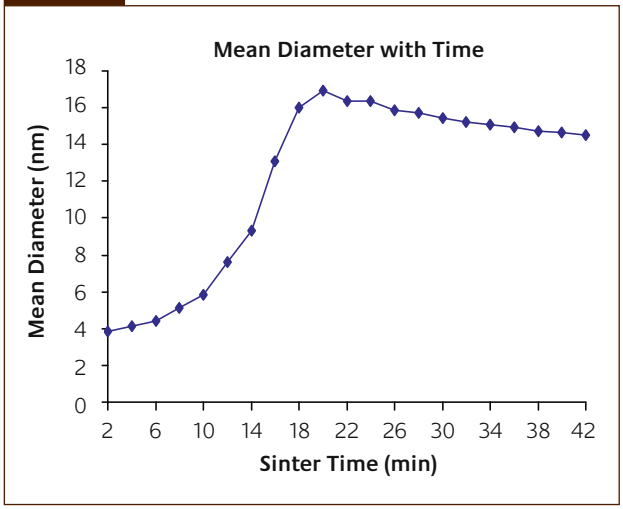

Plot of mean particle diameter with in-situ sinter time for particles with a 3nm starting size

grains during sintering. These are thought to be a small population of particles which are located on the reverse side of the support film that have relatively few neighbors with which to interact.

Figure 7 shows a time sequence of images showing the detailed densification behavior under electron beam irradiation of the 15nm particle preparation over a period of 56 minutes. The particle perimeters have been outlined in red for clarity, and it is apparent that the length of periphery and pore volume decrease progressively with sintering time. It is also clear, particularly in Figs 7(c) and (d) that recrystallization and grain growth phenomena are also occurring during densification.

Ex-situ sintering was performed by placing the membrane/nanoparticle sample, mounted in a TEM specimen holder, into an O_2(25%)-Ar plasma for two minutes. Samples were then returned to the JEOL 2000FX TEM for imaging. In contrast, to the behavior shown in Figure 3(a) and (b), the

Figure 7

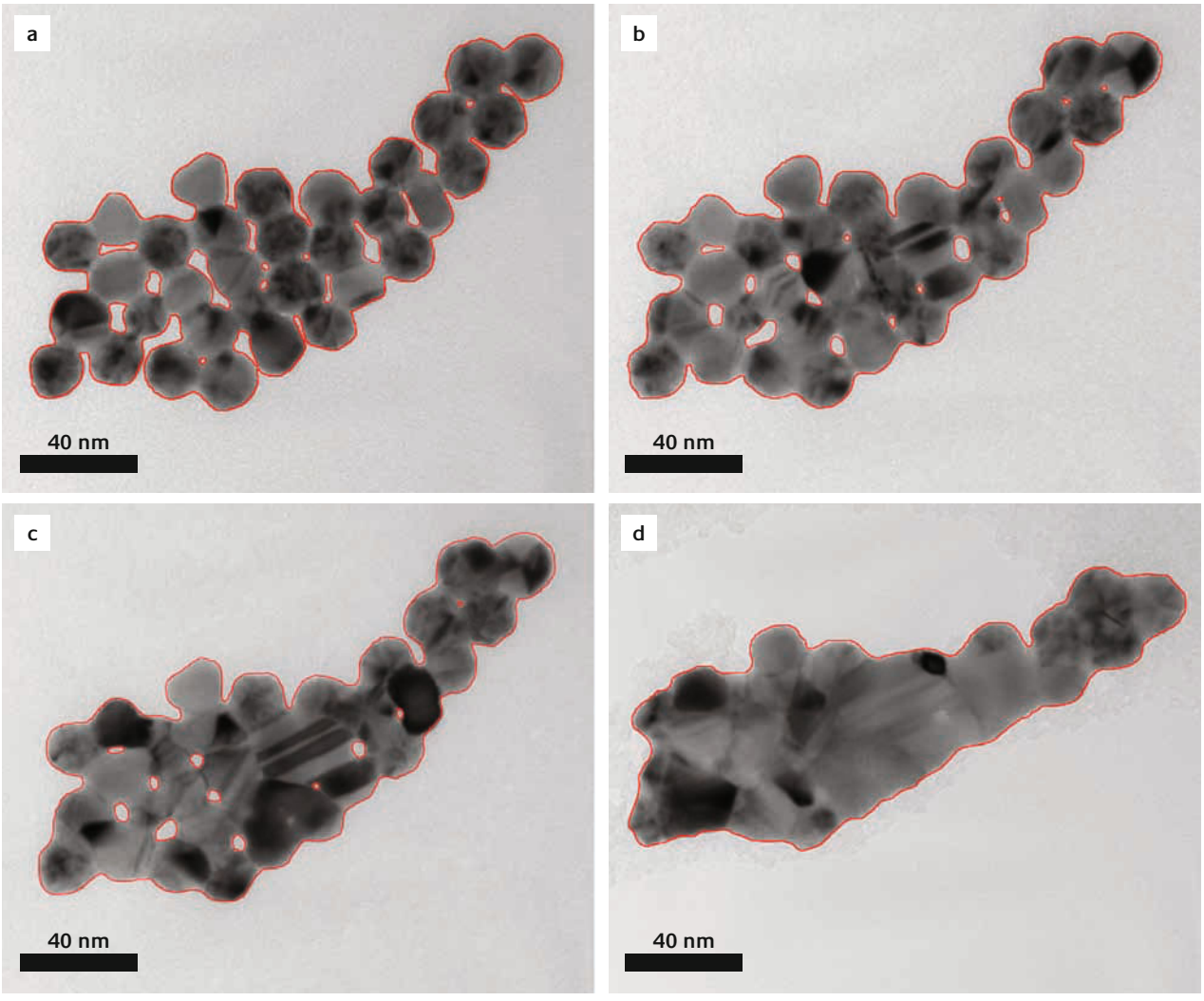

Sequence of micrographs showing the in-situ densification behavior of the 15nm particle preparation supported on a Si_3N_4 membrane. The images were captured after (a) 1 min, (b) 20 min, (c) 32 min and (d) 56 min of electron beam exposure [to a 300nm diameter spot with a current density of 50pA/nm^2]

Figure 8

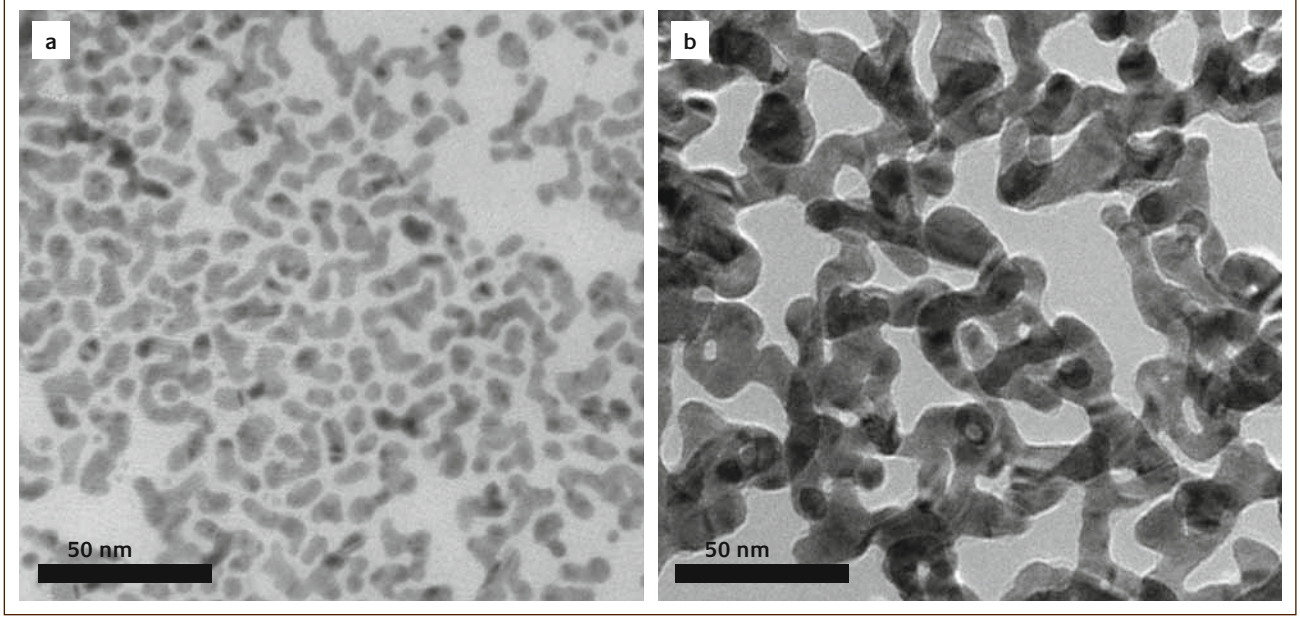

Rod or wire-like morphologies resulting from a rapid ex-situ oxygen/argon plasma sintering treatment of (a) the nominal 2nm and (b) 5nm preparations supported on Si_3N_4 membranes

2-nm particles rapidly sintered under oxygen-argon plasma conditions and had a final structure that differed greatly in appearance from the *in-situ* slow sintered sample. As can be seen from Figure 8(a) neighboring particles have connected up to form interlaced rod-type structures. Interestingly the diameter of the rods is relatively uniform at about 5nm and the structures show relatively little branching. It is also apparent that the Au seems to be wetting the Si_3N_4 substrate surface. Figure 8(b) shows that when the 5nm starting material is rapidly plasma sintered in the same manner, the resulting structure is much more connected and web-like, with a typical fiber thickness of about 10nm. The rapid-thermal sintering of nanoparticle arrays and lines on Si_3N_4 is being investigated further as an efficient method for the fabrication of nanopatterns and nanowires.

The effect of rapid thermal sintering in promoting an interconnected structure can be qualitatively understood by referring to Figure 9. An interconnected microstructure is favored when densification transport mechanisms (*e.g.* grain boundary diffusion) are rapid relative to coarsening transport mechanisms (*e.g.* surface diffusion). If the activation energy for densification is significantly greater than that for coarsening (which is consistent with the measured values for grain boundary and surface diffusion in gold), then a rapid heat up to a high enough temperature, such as that encouraged by plasma heating, will promote conditions favorable for densification relative to coarsening.

Classic experiments by Buffat and Borel [16,17] demonstrated that the melting temperature of Au particles decreases dramatically as the particle size decreases below 10 nm. The strong dependence of Au melting point with particle diameter, as calculated from the Buffat and Borel model [17], is shown in Figure 10. By implication, sub-10 nm-sized Au particles should readily sinter at temperatures much less than that required for larger particles. In fact, molecular dynamics simulations of nanoparticle sintering indicate that the mechanisms and kinetics differ significantly from micron-sized particle sintering [25]. To test whether sufficient driving

Figure 9

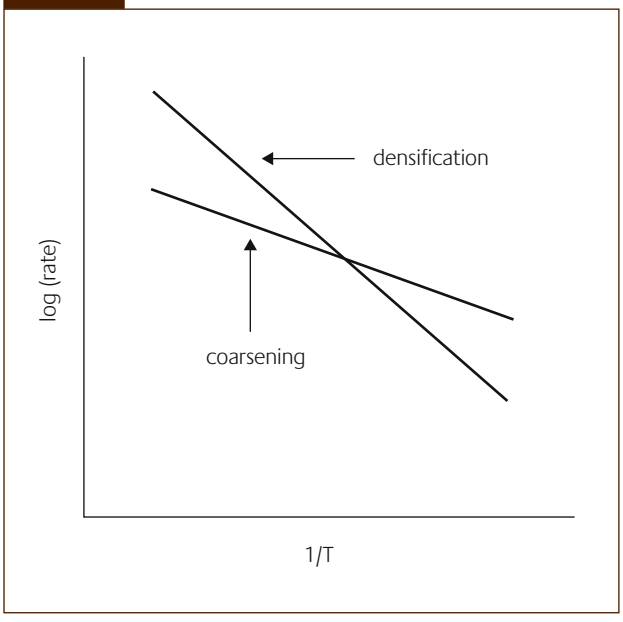

Schematic of the expected variation of coarsening and densification rate as a function of temperature. Densification is the preferred result of sintering at very high heating rates

Figure 10

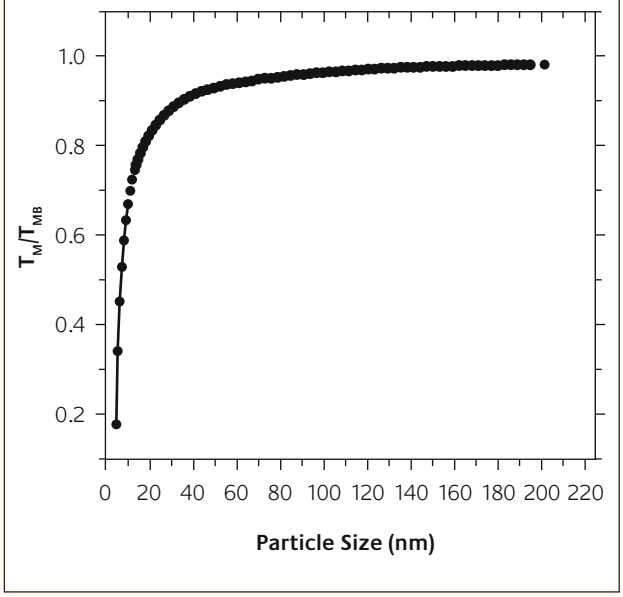

Calculated melting point depression (expressed as the ratio of nanoparticle melting temperature, T_M, to the melting point of bulk Au, T_{MB}) as a function of particle diameter

Figure 11

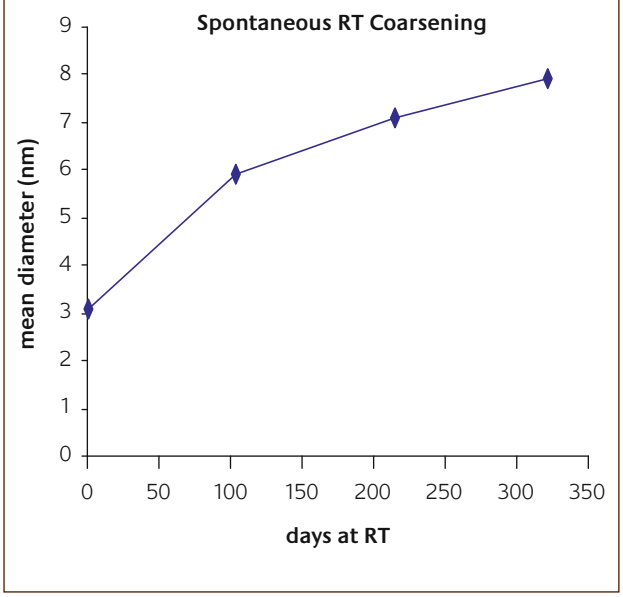

Plot of mean particle size as a function of room temperature (23±2°C) sintering time for a dried 3nm Au sample

Table 1

Summary of room temperature sintering data for different starting particle sizes

Average Particle Size at Start	Starting Areal Density	Sample Age	End Areal Density	Average Particle Size at End
(nm)	*(/10⁴ nm²)*	*(days)*	*(/10⁴ nm²)*	*(nm)*
2	480	214	29	7
3	432	147	67	7
4	396	154	336	4
5	201	151	200	5
15	37	147	37	15

force and mobility exist for nanoparticles to sinter at room temperature, a set of samples were deposited onto a Si_3N_4 substrate and stored under controlled ambient conditions at 23±2°C. These nanoparticle arrays were periodically observed by transmission electron microscopy over the course of one year. Other than periodic observation in a JEOL 2000FX TEM, these samples experienced no post-preparation processing.

Images of the 3 nm sample were recorded and mean particle size measured every ~100 days over a period of 300 days. A plot of mean size versus days since deposition (Figure 11) reveals a continuous increase in mean particle size, and a decrease in coarsening rate, with time. Table 1 shows that an obvious coarsening was observed in the 2nm sample as well, but samples with an initial mean particle size larger than 5 nm exhibited no change in size or areal particle density over 300 days. The 4 nm sample showed a very slight decrease in areal particle density, but no significant change in mean particle size. That these observations were due to spontaneous room-temperature sintering and not by interaction with the electron beam was evidenced by the fact that all areas of each sample showed the same stage of evolution over time. Another interesting feature that can be deduced from Table 1 is that in those samples which do exhibit room temperature sintering, particle growth ceases at around 7nm in diameter. This is presumably because the melting point of the particle has now increased to a point where surface diffusion has become insufficient to maintain growth at room temperature. Furthermore, these room temperature sintering results imply that the dodecane-thiol protective ligand shell on the 2 and 3 nm Au nanoparticles must have been more significantly compromised than for the corresponding 4, 5 and 8 nm particles.

Conclusions

This work has allowed us to gain a first overview of the factors that affect the sintering of Au nanoparticles. We have shown that arrays of smaller Au particles (2-8 nm) exhibit a fundamentally different sintering behavior on Si_3N_4 substrates as compared to larger 15nm particles (*i.e.* coarsening as compared to densification). This difference may be due to a combination of more strongly bound ligands and a larger particle radius to particle separation (R/S) for the 15nm particles. In addition, for the smaller nanoparticles, the rate at which the arrays are heated strongly influences the type of sintered morphology obtained, with slow heating giving rise to more spherical coarsened clusters and rapid heating resulting in highly interconnected string-like structures. We find also that Au nanoparticles below 4 nm in diameter can spontaneously sinter in the dried out state at room temperature over extended time periods, probably as a consequence of ligand destabilization and their depressed melting points. This room temperature sintering phenomena ceases however when the particle has grown to a size of about 7nm suggesting that the size-dependant melting point of the material is an important factor to consider in this process. This phenomenon, although specific to Si_3N_4 supports at present, could have far reaching consequences for the long-term stability of self-assembled devices constructed with sub-4 nm Au particles in which the device function depends on retaining the structural integrity of the individual particles over long time periods.

Acknowledgements

CJK and MPH would like to acknowledge the financial support of the NSF (grants# DMI-0304180 and DMI-0457602) and the Pennsylvania Department of Community and Economic Development under contract # 20-906-0009.

About the authors

Chris Kiely is Director of the Nanocharacterization Laboratory and a Professor of Materials Science and Engineering at Lehigh University, USA. His research expertise lies in the application and development of transmission electron microscopy techniques for the study of nanoscale features in materials. Particular areas of interest include catalyst materials, nanoparticle self-assembly, carbonaceous materials, and heteroepitaxial interface structures. He is also involved in microscopy technique development, and his current interests include X-Ray ultra-Microscopy (XuM) and aberration corrected Analytical Electron Microscopy (AEM).

Mathias Brust is a Professor in the Department of Chemistry at the University of Liverpool, UK. He has worked with gold nanoparticles for over 15 years, and his most important contributions to the field relate to particles' synthesis and functionalization, and to nanostructure self-assembly. His current interests include the design and preparation of nanoparticle bioconjugates for diagnostics, controlled delivery and other purposes, for example to study and manipulate their interactions with living cells.

References

1 E.A. Dobisz, F.A. Buot and C.R.K. Marrian; A.S. Edelstein, R.D. Cammarata, *eds*., Institute of Physics Publishing, Bristol and Philadelphia, 1996
2 D. Eigler, *Solid State Communications*, 1998, **107**, 711
3 R.D. Piner, J. Zhu, F. Xu, S. Hong and C.A. Mirkin, *Science*. 1999, **283**, 661
4 A. Terfort, N. Bowden and G.M. Whitesides, *Nature*, 1997, **386**, 162
5 N. Bowden, A. Terfort, J. Carbeck and G.M. Whitesides, *Science*. 1997, **276**, 233
6 M. Brust and C.J. Kiely, *Colloids and Surfaces*. 2002, **202**, 175
7 G. Schmid, *Chem. Rev.* 1992, **92**, 1709
8 M. Brust, D. Bethell, D. Schiffrin and C.J. Kiely, *Adv. Mater*., 1995, **7**, 795
9 C.B. Murray, C.R. Kagan and M.G. Bawendi, *Science*, 1995, **270**, 1335
10 R.P. Andres, J.D. Bielefeld, J.I. Henderson, J.B. Janes, V.R. Kolungunta, C.P. Kubiak, W.J. Mahoney and R.G. Osifchin, *Science*, 1996, **273**, 1690
11 Z.L. Wang, *Adv. Mater*., 1998, **10**, 13
12 M. Brust, M. Walker, D. Bethell, D.J. Schiffrin and R. Whyman; *J. Chem. Soc. Chem. Commun*., 1994, 801
13 Y. Chen, R.E. Palmer and J.P. Wilcoxon, *Langmuir*, 2006, **22**, 2851
14 C.J. Kiely, J. Fink, M. Brust, D. Bethell and D.J. Schiffrin, *Nature*, 1998, **396**, 444

15 T.O. Hutchinson, Y.P. Liu, C. Kiely, C.J. Kiely and M. Brust, *Adv. Mats*., 2001, **13**, 1800

16 P. Buffat and J-P. Borel, *Phys. Rev. A*, 1975, **13**, 2287

17 P. Buffat, *Thin Solid Films*, 1976, **32**, 283

18 P.R. Couchman and W.A. Jesser, *Nature*, 1977, **269**, 481

19 J.P. Borel, *Surface Science*, 1981, **106**, 1

20 R.R. Vanfleet and J.M. Mochel, *Surface Science*, 1995, **341**, 40

21 S. Iijima and T. Ichi, *Phys. Rev. Letts*., 1986, **36**, 616

22 J.R. Sambles, *Proc. Roy. Soc. A*, 1971, **325**, 339

23. M. Flueli, P.A. Buffat and J.P. Borel, *Surface Science*, 1988, **202**, 343

24. H.B. Liu, M. Jose-Yacaman, R. Perez and J.A. Ascensio, *Appl. Phys, A*., 2003, **77**, 63

25 P. Zeng, S. Zajac, P.C. Clapp and J.A. Rifkin, *Mat. Sci. and Eng,*. 1998, **A252**, 301

26 K. Nakaso, M. Shimada, K. Okuyama and K. Deppert, *J. Aerosol Sci,*. 2002, **33**, 1061

27 S. Arcidiacono, N.R. Bieri, D. Poulikakos and C.P. Grigoropoulos, *J. Multiphase Flow*, 2004, **30**, 70

28 T. Hawa and M.R. Zacharia, *J. Aerosol Sci*., 2006, **37**, 1

29 L.J. Lewis, P. Jensen and J.L. Barrat, *Phys. Rev. B*, 1997, **56**, 2248

30 M.J. Hostetler, J.E. Wingate, C-J. Zhong, J.E Harris, R.W. Vachet, M.R Clark, J.D. Londono, S.J. Green, J.J. Stokes, G.D. Wignall, G.L.Glish, M.D. Porter, N.D Evans, and R.W Murray, *Langmuir*, 1998, **14**, 17

31 I. Hussain, M. Brust, A. Papworth and A.I. Cooper, *Langmuir*, 2003, **19**, 4831

32 D.V. Leff, L. Brandt and J.R. Heath, *Langmuir*, 1996, **12**, 4723

33 R.H. Terrill, T.A. Postlethwaite, C. Chen, J.E. Hutchison, C. Poon, A. Tarzis, A. Chen, M.R. Clark, C.S. Johnson, E.T. Samulski, J.M. Desimone and R.W. Murray, *Abstr. Papers Am. Chem. Soc*., 1995, **210**, 380

34 M.K. Corbiere, N.S. Cameron and R.B. Lennox, *Langmuir*, 2004, **20**, 2867